

**MELT INCLUSION, TRACE ELEMENT, AND ISOTOPIC ANALYSES OF A POIKILITIC SHERGOTTITE SUITE: IMPLICATIONS FOR MARTIAN MAGMATISM** E. W. O'Neal<sup>1</sup>, A. M. Ostwald<sup>1</sup>, A. Udry<sup>1</sup>, J. Gross<sup>2</sup>, M. Richter<sup>3</sup>, D. R. McQuaig<sup>3</sup>, T. J. Lapen<sup>3</sup>, G. H. Howarth<sup>4</sup> and R. Johnsen<sup>1</sup> <sup>1</sup>Department of Geoscience, University of Nevada Las Vegas, 4505 S. Maryland Pkwy, Las Vegas, NV 89154-4010, oneal1@unlv.nevada.edu; <sup>2</sup>Department of Earth and Planetary Sciences, Rutgers University, Piscataway, NJ 08854, USA; <sup>3</sup>Department of Earth and Atmospheric Sciences, University of Houston, Houston, Texas 77204; <sup>4</sup>Department of Geological Sciences, University of Cape Town, Rondebosch 7701, South Africa

**Introduction:** The most common type of martian meteorites, making up ~90% of the martian meteorite collection, are the shergottites, which are classified as basaltic, olivine-phyric, poikilitic, and gabbroic based on texture and mineralogy. The poikilitic shergottites are the most abundant, comprising more than 20% of the martian meteorite collection [1,2]. Geochemically, poikilitic shergottites can be classified as enriched, intermediate, and depleted based on light rare earth element abundances and isotopic compositions.

Poikilitic shergottites are crucial to the study and understanding of martian magmatism and geological history, as they likely represent a major lithology of the martian crust [2-5]. Their unique bimodal texture separates the poikilitic shergottites from the other shergottite subgroups. This bimodal texture can display the entire evolution of poikilitic shergottites as the early stage poikilitic texture (domain 1) is representative of slow cooling at depth, and the non-poikilitic late-stage interstitial texture (domain 2) is reflective of magma ascent and more rapid cooling [2,4].

We conducted major and trace element melt inclusions (MI) analyses to better constrain parental magma compositions, as the melt evolves from one domain to another, while also examining potential crustal contamination in the melt [2,4]. Through <sup>176</sup>Lu/<sup>177</sup>Hf and <sup>147</sup>Sm/<sup>143</sup>Nd isotopic analyses, we are working on determining crystallization ages for two poikilitic shergottites, which will constrain time of formation, sources, and therefore potential distribution of the shergottite suite on Mars.

**Methods:** We conducted MI analysis on five poikilitic shergottites: two are enriched (Northwest Africa [NWA] 7755 and NWA 10618), and three are intermediate (NWA 11065, NWA 11043, Allan Hills [ALHA] 77005). Backscatter-electron (BSE) images were taken of a thin section for each sample using the JEOL JSM-5610 scanning electron microscope (SEM) at University of Las Vegas, Nevada (UNLV) to identify MI and their phases throughout the bimodal textures (Fig. 1). We conducted *in situ* major and minor elemental analyses of the MI using Rutgers University JEOL JXA-8200 Superprobe electron probe micro-analyzer (EPMA). To get an accurate measurement of the present bulk composition (PBC) of each MI, we calculated the volumetrically-weighted average for each sample's mineral

phases. Modal abundances were calculated with *ImageJ* software by point counting phases in BSE images. Modal abundance values were normalized and multiplied by the average composition of each phase. Using the PBCs, we calculated the parental trapped liquid (PTL) compositions for each MI using *Petrolog3* [4] as this software corrects for post entrapment processes (including diffusion) [7]. We used MELTS software to account for 'Fe-Mg' loss [4,7,8].

*In situ* analyses of trace elements within the MI were conducted at UNLV using the UNLV ESI 193 nm Excimer NWR193 laser ablation system, which is coupled with an iCAPTM Qc ICP-MS. We used a 100 µm laser spot size for MI < 100 µm; for MI with diameters larger than 100 µm, we took multiple points to encompass the entire MI and then averaged results. The laser was kept at a frequency of 5 Hz, and a fluence of 4 J/cm. Measurements were taken with a background time of 10 s, an ablation time of 50 s, and a washout time of 5 s. NIST 610 and BHVO were used as standards. Data reduction was performed using *Iolite4* [17].

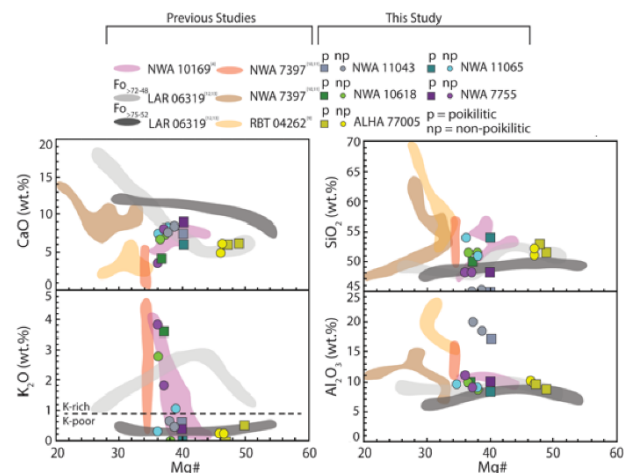


**Figure 1:** Mg# of calculated PTL compositions from melt inclusions versus K<sub>2</sub>O, CaO, Al<sub>2</sub>O<sub>3</sub>, and SiO<sub>2</sub>, for shergottites. Intermediate poikilitic shergottite PTL compositions: NWA 11065, NWA 11043, and ALHA 77005; enriched poikilitic shergottite PTL compositions: NWA 10618, NWA 7755, RBT 04262 [9], NWA 7397 [10,11], and NWA 10169 [4]; enriched olivine-phyric shergottite PTL composition: LAR 06319 [12,13]. p = poikilitic np = non-poikilitic.

<sup>176</sup>Lu/<sup>177</sup>Hf and <sup>147</sup>Sm/<sup>143</sup>Nd isotopic analyses were conducted on two poikilitic shergottites: NWA 7755 and NWA 11043. We follow the methods of [4] for min-

eral separation. Mineral fractions were then sent to University of Houston, where they were spiked and prepared for Inductively Coupled Plasma-Mass Spectrometry (ICP-MS) following the techniques presented in [14,15]. The isotope ratios were analyzed using a Nu Instruments II MC-ICP-MS following the procedures outlined in Combs et al. (2019) [4].

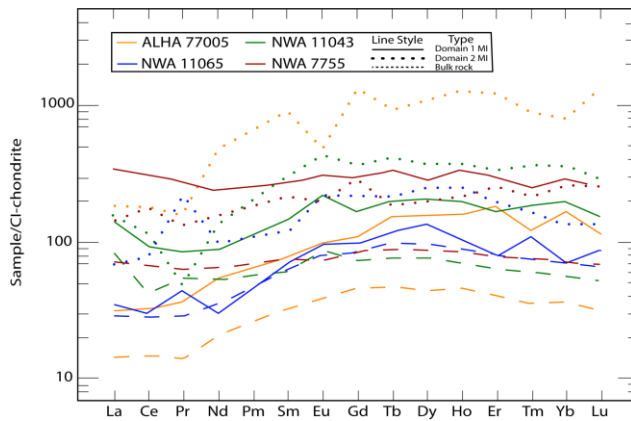


**Figure 2:** REE profiles of MI from domains 1 and 2 from our study compared to the bulk rock REE profiles of said shergottites from previous studies [5,16]. Full colored lines represent MI from domain 1. Dotted lines represent MI from domain 2. Dashed lines represent bulk rock.

**Results:** Melt inclusion analysis comprises six olivine-hosted MI in domain 1, and seven MI in domain 2. The average size of these MI is  $\sim 120 \mu\text{m}$  with the largest MI at  $400 \mu\text{m}$  and the smallest at  $50 \mu\text{m}$ . There is no observed correlation between MI size and texture. All analyzed MI are polyminerallitic, and include phases such as glass, pyroxene, phosphates, oxides, and sulfides. All MI have a feldspathic glass phase, while some MI also exhibit another homogeneous high-silica glass phase along with the feldspathic glass (Fig. 1). Some feldspathic glass phases are enriched in potassium (K). The olivine hosts of the MI have compositions of  $\text{Fo}_{57-71}$ . The  $\text{Mg\#}$  [=  $100 \times \text{molar MgO}/(\text{MgO} + \text{FeO})$ ] for the MI in domain 1 in the suite is  $\sim 40-50$ , while the  $\text{Mg\#}$  in domain 2 MI is  $\sim 35-47$ . Potassium enrichment ( $>1 \text{ K}_2\text{O wt.}\%$ ) is seen in MI in domain 1 ( $n=1$ ) and domain 2 ( $n=4$ ). Melt inclusions in domain 1 and 2 exhibit similar  $\text{CaO}$  contents ranging from  $3-10 \text{ wt.}\%$ . The  $\text{Al}_2\text{O}_3$  content generally shows an increase from MI in domain 1 ( $\sim 8-16 \text{ wt.}\%$ ) to MI in domain 2 ( $\sim 9-21 \text{ wt.}\%$ ). The  $\text{SiO}_2$  measured in MI in domain 1 and 2 is the same ( $\sim 40-55 \text{ wt.}\%$ ). The  $\text{K}_2\text{O}/\text{Na}_2\text{O}$  is variable ( $\sim 0.02-1.9$ ) throughout the MI in both domains (Fig. 1).

One MI from each domain in each meteorite was selected for *in situ* analyses of trace elements for a total of 10 MI. Rare earth element diagram (Fig. 2) show parallel plots between the MI trace elements and bulk rock trace elements for all shergottites. La/Lu variability is seen in ALHA 77005 ( $0.13-0.45$ ) and NWA 11043

( $0.54-1.65$ ) and is more prevalent in domain 2 MI. At the time of submitting this abstract our isotopic analysis results are still being processed.

The  $^{176}\text{Lu}/^{177}\text{Hf}$  versus  $^{176}\text{Hf}/^{177}\text{Hf}$  5-point isochron yielded a crystallization age of  $223 \pm 46 \text{ Ma}$  ( $\text{MSWD} = 0.24$ ), and an initial  $^{176}\text{Hf}/^{177}\text{Hf}$  ratio of  $0.282167 \pm 0.00001$  for NWA 7755.

**Discussion and conclusions:** The overlap of the poikilitic shergottite PTL compositions with the olivine-phyric PTL composition ranges suggest that poikilitic shergottites and olivine-phyric shergottites may share a petrological link and similar petrogenesis/magmatic history. The PTL compositions of poikilitic shergottites are not as primitive and cover a smaller  $\text{Mg\#}$  range ( $\sim 36-50$ ) than that of the olivine-phyric PTL ranges ( $\sim 20-56$ ) (Fig. 1).

The variability of  $\text{K}_2\text{O}/\text{Na}_2\text{O}$  ratio between the samples suggest that poikilitic shergottites may go through a common process during melt evolution resulting in the addition of K-rich metasomatized material, which is evident in this study and previous studies [4,9]. Therefore, the K-enrichment is likely a result of assimilation or alteration in the crust, and not by a metasomatized mantle source or fractionation of K-poor mineral phases. Generally the K-rich melt inclusions in our study have  $\text{K}_2\text{O}/\text{Na}_2\text{O}$  ratios  $>1.0 \text{ wt.}\%$ , while all the K-poor melt inclusions have  $\text{K}_2\text{O}/\text{Na}_2\text{O}$  ratios  $<1.0 \text{ wt.}\%$  indicating that the K-enrichment is likely inherited from an enriched source or occurs during a magmatic process.

The parallel rare earth element profiles of the MI compared to bulk rock (Fig. 2) suggest that the MI are all sampling melts from a single source. La/Lu will vary from MI to MI and differ from bulk La/Lu because La and Lu have different compatibilities in olivine. Different compatibility mean different diffusion rates for the MI into host olivine. Lack of variability of La/Lu in the shergottites suggests that these MI are not heavily reequilibrated post-crystallization, likely forming in a closed system. The variability of La/Lu in ALHA 77005 and NWA 11043 is possibly due to diffusive reequilibration occurring in an open system [18].

**References** [1] Goodrich, C. A. (2002) *MAPS*, 37, B31-B34. [2] Howarth G. H. et al., (2014) *MAPS*, 49, 1812-1830. [3] McSweeney H. Y. (2015) *Am. Min.* 100(11-12), 2380-2395. [4] Combs, L. M. et al., (2019) *GCA*, 266, 435-462. [5] Rahib, R. R. et al., (2019) *GCA*, 266, 463-496. [6] Danyushevsky, L. V. (2000) *Contrib. Mineral. Petrol.*, 138(1), 68-83. [7] Danyushevsky, L. V. & Plechov, P. (2011) *Geochem. Geophys. Geosys.*, 12(7). [8] Filiberto, J. & Dasgupta R. (2011), *Earth Planet. Sci. Lett.* 304, 527-537. [9] Potter et al., (2015) *LPSC XXXXVI, Abstract #2889*. [10] Ferdous et al., (2018) *LPSC XLIX, Abstract #2083*. [11] He Q. and Xiao L., (2014) *LPSC XXXV, Abstract #1668*. [12] Peslier et al., (2010) *MAPS*, 74, 4543-4576. [13] Basu Sarbadhikari et al., (2011) *GCA* 75, 6803-6820. [14] Munker et al., (2001) *Geochem. Geophys. Geosys* (2) [15] Lapen et al., (2004) *Geochem. Geophys. Geosys* (5) [16] Lodders (1998) *Met. Planet. Sci.* 33(4): A183-A190. [17] Paton et al., (2011) *J. Anal. At. Spectrom.* [18] Cottrell et al., (2002) *Geochem. Geophys. Geosys*